Analysis of high frequency oscillations in voltage transformer

Y. Shibuya, K. Wada, H. Muto

Abstract-- The voltage transformers (VTs) used in medium voltage circuit have a large number of turns more than 10000. They are reported to be sometimes vulnerable to fast rising abnormal voltages due to lightnings or switchings. It has been regarded difficult to analyse such a high frequency phenomenon in the VT because of the large number of turns.

A high frequency model of VT is obtained in a form of lumped constant circuit, and is analysed using the Fast Fourier Transform (FFT). The circuit constants of model are calculated from the winding specification data based on turn-to-turn basis, but the circuit is analysed in terms of multiple-turn groups reducing the order of equations to a manageable level. The dissipation related constants are introduced in the equivalent circuit considering the skin and proximity effects in the conductors as well as the dielectric loss in the insulation.

Firstly, the state equation of VT model circuit is solved for a range of FFT frequencies. Then, the time domain analysis is performed using the inverse FFT technique. Both the frequency and time domain characteristics are verified by the experiment on an actual 6.6 kV VT, in which internal voltage oscillations are observed through taps. The general tendencies of high frequency oscillations are investigated using a simpler model. It is found the interlayer insulation near the input terminal is disproportionally highly stressed for impulses with fast rise time.

The proposed analysis is considered to be useful since it can be performed when the geometrical specifications of VT are available.

Keywords: Voltage transformer, High frequency, Oscillation, Winding, FFT

I. Introduction

A lot of voltage transformers (VTs) are used not only in the utilities' substations but also in the users' entrance terminal areas. Particularly, enormous number of them are used in high voltage distribution systems. Although those VTs are designed to withstand abnormal voltages anticipated in the system, their damages in the field have been still reported [1]. It is suggested that a layer-short occurs probably because of fast rising surges originated from the lightning or switching operation especially of a vacuum circuit breaker.

This phenomenon is considered to be essentially same as the voltage oscillations which have been studied extensively in power transformers [2]. However, the analysis of voltage oscillations in VT has been not attempted probably because the number of turns is much larger than the ordinary transformers.

The authors have successfully applied the technique used in the ordinary transformers to the high frequency transients in VT [3]. However, it has been recognised that the dissipation at high frequencies was not adequately represented in the previous analysis. In the present analysis, the proximity effect is newly incorporated in a manageable manner in addition to the skin effect and the dielectric loss.

II. Circuit Model of VT

A. Construction of VT

Most VTs commonly used in distribution system have the configuration shown in Fig. 1. The high voltage (HV) or primary winding is composed of turns wound in many layers. PET films are used both in the layer and main insulations. The main insulation refers to the space between HV and in the low voltage (LV) windings.

The beginning and end terminals of HV winding are denoted as V and U here, respectively. A surge is assumed to be applied to either V or U, while the other terminal is at the ground potential. The voltages of core and LV winding are also set to be zero in the present analysis.

B. Equivalent circuit

The lumped constant circuit shown in Fig. 2 is used in the analysis. Dividing HV winding into N groups defines N +1 nodes. Inductances and capacitances between these nodes are expressed in the matrices [L] and [C] [3]-[4]. The resistance

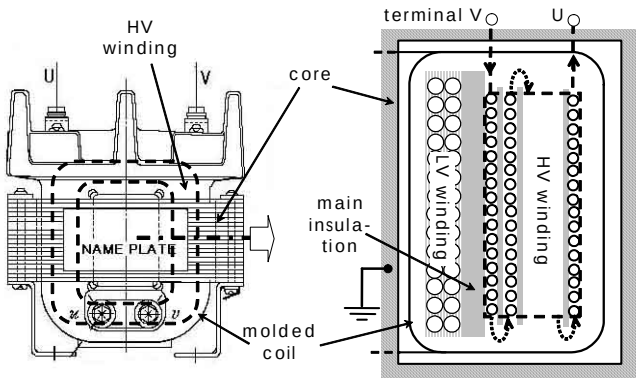

(a) Outside view (b) Cross-section of coil

Fig.1. Configuration of voltage transformer.

Y. Shibuya is with Shibaura Institute of Technology, Koto-ku, Tokyo, Japan (e-mail of corresponding author: shibuya@sic.shibaura-it.ac.jp).
K. Wada and H. Muto are with Mitsubishi Electric Corp., Amagasaki, Hyogo, Japan (e-mails: Wada.Kotaro@dp.MitsubishiElectric.co.jp and Muto. Hirotaka@da.MitsubishiElectric.co.jp)

Presented at the International Conference on Power Systems Transients (IPST'07) in Lyon, France on June 4-7, 2007

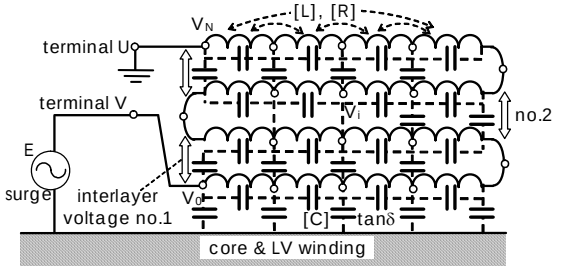

Fig. 2. Equivalent circuit.

matrix [*R*] represents the dissipation due to the skin and proximity effects [5]. Dielectric dissipation is defined by tanδ for each capacitance.

Incoming surge is represented by a sinusoidal voltage *E* in frequency analysis. In Fig. 2, the voltage is applied at terminal V, terminal U being grounded.

C. Basic equations

The interconnected circuit shown in Fig. 2 has been analysed using matrices [2]-[6]. It is possible to get the state equation for the nodal voltage (*V*) in the following form [6].

$$[A](V) = (E) \tag{1}$$

Where, (*E*) is a vector including *E*, and [*A*] can be obtained from the impedance and admittance matrices [*Z*] and [*Y*]:

$$\begin{cases} [Z] = j\omega[L] + [R] \\ [Y] = j\omega[(1 - j\tan\delta)C] \end{cases} \tag{2}$$

In the FFT analysis, the solution of (1) has to be obtained for a number of frequencies ω.

III. Determination of Constants

The circuit parameters [*L*], [*C*] and [*R*] are directly obtained from the geometry data of VT on electromagnetic principles. Those calculated on turn-to-turn basis can be distributed among the groups of turns just in the way employed previously in core-type transformers [4], [7].

A. Turn-to-turn inductances

The inductances are calculated ignoring the presence of core considering the analysis in high frequencies. The self inductance is calculated by a parallel wire approximation and the mutual by two coaxial rings approximation [3].

B. Turn-to-turn capacitances

Capacitances are assumed only at interturns facing each other or at turns directly facing the ground. The parallel plate capacitance approximation is used in the evaluation, considering the dielectric constant of the relevant space [3].

C. Resistance matrix

The matrix [*R*] represents the loss related to eddy currents in conductors. One part of them is produced by the current flowing in its own conductor, and another part is produced by the currents in other conductors. They are called skin and proximity effects, respectively. The latter becomes dominant ar high frequencies, especially in the case the number of turns is large [5]. Therefore, [*R*] is expressed as follows.

$$[R] = [R_{\text{skin}}] + [R_{\text{prox}}] \tag{3}$$

The diagonal matrix $[R_{\text{skin}}]$ is evaluated using the formula for the inductance of circular cross-section conductor [5].

$$\left[R_{\text{skin}}\right]_{ii} = \text{Re}\left[\frac{\alpha}{2\pi a\sigma}\cdot\frac{I_0[\alpha a]}{I_1[\alpha a]}\right]\cdot\ell_i \quad \left(\alpha = \sqrt{j\omega\mu_0}\right) \tag{4}$$

Where, *a*, σ and ℓ_i are the conductor's radius, conductivity, and length of the group. μ_0 denotes the permeability of vacuum, and I_n, the modified Bessel functions of the first kind and order *n*.

The element of $[R_{\text{prox}}]$ is given in the form [5]:

$$[R_{\text{prox}}]_{ij} = \sum_{m=1\,(m\neq i,\,j)}^{N} F_m(\omega)\cdot\ell_m\cdot\left(f_{rm}^{i}\cdot f_{rm}^{j} + f_{zm}^{i}\cdot f_{zm}^{j}\right) \tag{5}$$

Where, f_{rm}^{i} and f_{zm}^{i} are the coefficients defined by the relation that the radial and axial magnetic fields at group *m* produced by current *I* at group *i* are given by $H_r = f_{rm}^{i} I$ and $H_z = f_{zm}^{i} I$, respectively. Here, the axi-symmetry is assumed. Those field coefficients can be determined from the winding geometry. The function $F_m(\omega)$ indicates the loss per unit length of conductor in the presence of unit magnetic field of frequency ω. In the case of circular cross-section wire, the following expression is used.

$$F_m(\omega) = \text{Re}\left[\pi a\sqrt{\frac{j\mu_0}{\sigma}}\,\tanh\frac{\pi a\sqrt{j\sigma\mu_0\omega}}{4}\right] \tag{6}$$

This is converted from the expression for rectangular cross-section conductor given in reference [5].

D. Fast calculation of Resistance matrix

It is found that executing the calculation of $[R_{\text{prox}}]$ by (5) is prohibitingly slow. The following bold approximations are made to reduce the calculation time to a practically manageable level.

Firstly, $F_m(\omega)$ and ℓ_m in (5) are respectively approximated by $\overline{F}(\omega)$ and $\overline{\ell}$; their averages for *m*=1, ⋯ , *N*. Then, $[R_{\text{prox}}]$ is expressed in a simpler form:

$$[R_{\text{prox}}] = \overline{F}(\omega)\cdot\overline{\ell}\cdot[F_{rz}] \tag{7}$$

Where, matrix $[F_{rz}]$ is composed of the elements: $\sum_{m=1\,(m\neq i,\,j)}^{N}(f_{rm}^{i}\cdot f_{rm}^{j} + f_{zm}^{i}\cdot f_{zm}^{j})$, which is independent of frequency.

The diagonal elements of $[F_{rz}]$ are found to be much larger than the nondiagonal. In the present analysis, the diagonal components are calculated individually, but all the nondiagonal elements are set to the average value obtained at the winding centre i.e. $(\sum_{j=1}^{N}[F_{rz}]_{N/2\,j})/N$. This will be justified considering that the total amount of elements of [*R*] is effective for high frequency dissipation.

IV. Conditions of Analyses

A. Examples of VTs

The two examples of VTs shown in Table I are analysed. Model C is for calculation only, and Model A is for actual VT of 6.6 kV, 50 VA.

TABLE I
ANALYSED VTS

	Model C (for calculation)		Model A (6.6kV VT)	
interturn spacing (mm)	0.16		0.05 – 0.08	
no. of layers	10		44	
no. of turns per layer	100		68 – 244	
no. of groups	100	1000	1031	2062
av. length in a group (m)	5.06	0.51	5.24	2.67

Following physical parameters are used:

conductor conductivity $\sigma=5\times10^7$ S/m,

interlayer space dielectric constant and loss tangent

$\varepsilon_s=2.1$, $\tan\delta=0.05$.

Although the total number of turns of Model A is about 10 times larger than that of Model C, the average length in a group of Model C of 100 groups is similar to that of Model A of 1031 groups. Fig. 3 shows the cross-sectional view of Model C with 100 groups, the node points indicated by circles.

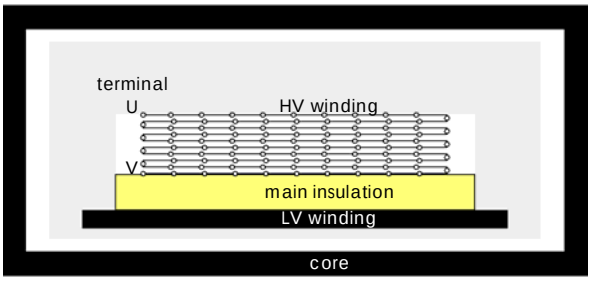

Fig. 3. Cross-sectional view of Model C with 100 groups.

B. FFT analysis

Frequency characteristic is readily obtained by solving (1) for a range of frequencies. The response to input voltage of arbitrary waveform can be analysed using the inverse FFT technique.

In preparation, the solution of (1) or complex voltage (V) is calculated at a series of Fourier frequencies:

$$f = 0,\ f_0,\ 2f_0,\ \cdots,\ nf_0\ (=f_m)$$

Then, the inverse FFT technique [7] provides the means to calculate the voltages induced by any input at the times:

$$t = 0,\ t_0,\ 2t_0,\ \cdots,\ 2nt_0\ (=T)$$

The following relations hold:

$$t_0 = 1/(2f_m),\quad T = 1/f_0 \tag{8}$$

In most of the present FFT analyses, the following constants are used:

f_0 = 78 kHz, f_m = 40 MHz, n = 512,

t_0 = 12.5 ns, T = 12.8 μs

The values of n and f_m are increased accordingly if higher time resolutions are needed.

C. Experimental

Frequency and time domain characteristics are verified by the experiment on the 6.6 kV, 50 VA VT corresponding to Model A. Frequency characteristic of terminal impedance is measured using a network analyzer.

As for time domain experiment, unipolar impulses having rise times ranging from 50 ns to 1μs are generated using IGBT switch, and applied to VT terminal either V or U. Induced interlayer voltages are observed through prefabricated taps using a high impedance differential probe connected to oscilloscope.

V. Frequency Domain Analyses

A. Amount of grouping

Modelling with large number of groups requires a long computation time, particularly when it exceeds 1000. It is necessary to know what amount of grouping is sufficient for a given problem.

Fig. 4 shows how the frequency characteristic of Model C varies with different numbers of grouping: 100 and 1000. As shown in Table I, the average lengths of group differ 10 times. It is suggested that the upper limit frequency simulated by the model using the group length ℓ is given by [3] :

$$f_{max} = v_s/(2\ell) \tag{9}$$

Where, v_s is the surge velocity in the winding. The dielectric constant of interlayer space $\varepsilon_s=2.1$ indicates v_s =207 m/μs. Then, the above two cases correspond to f_{max} = 20 and 200 MHz, which accords with Fig. 4.

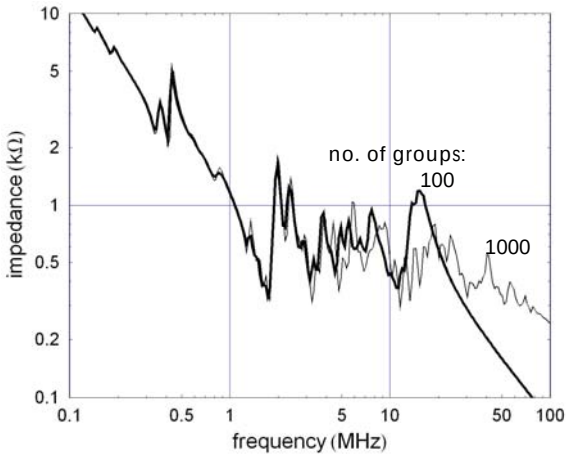

Fig. 4. Frequency characteristics of impedance at terminal V for Model C analysed with different numbers of groups.

B. Comparison with experiment

In Fig. 5, the analysed results of Model A are compared with the experimental. They agree relatively well in the wide frequency range. In the curve of 1031 groupings, resonances are seen at around 25 MHz, which is thought to be the upper

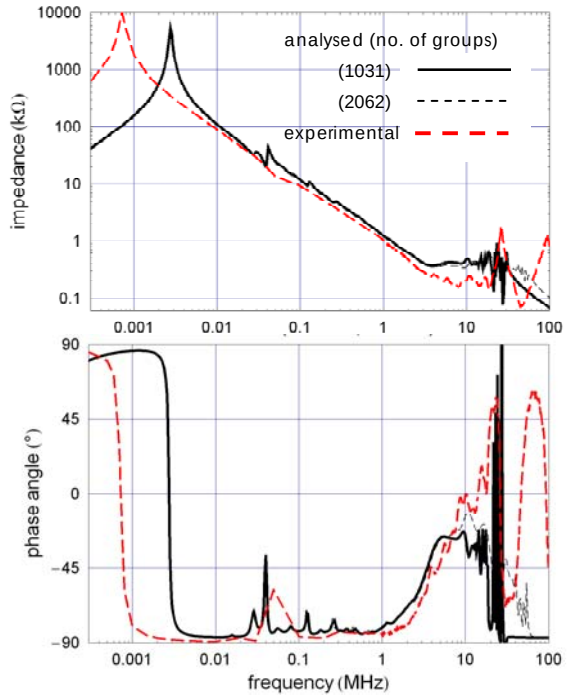

Fig. 5. Frequency characteristics of impedance at terminal V for Model C.

limit as mentioned above. The ups and downs at this frequency may indicate that the grouping number is not sufficient. Indeed, the resonance at this frequency is much subdued in the analysis with 2062 grouping. In the calculations below, the model with 1031 groups is mostly used as far as the result is reasonable.

A similar correspondence is observed in the frequency characteristics of impedance for terminal U.

C. Voltage distribution

When a sinusoidal voltage is applied to VT, some voltage is induced at every node, so that the voltage is distributed along whole winding. The voltage distribution at low frequencies is uniform or linear, but it departs from the linear distribution at high frequencies.

Fig. 6 shows the voltage distribution in the case that 1 MHz sinusoidal voltage is applied to Model C. Both of the two curves (voltage applied terminal: V or U) are not smooth linear distributions. The nonlinearity becomes more pronounced at high frequencies. This is the problem that some interlayer insulation can be stressed disproportionally.

Fig. 7 shows how the interturn voltage distributes inside the HV winding in the case that 1 MHz sinusoidal voltage is applied to terminal V of Model C. In this case, interlayer voltages at various points are displayed on the plane showing the interlayer location.

According to Fig. 7, the interlayer voltage tends to become large at the edge of layer. However, it is noticed that the interlayer voltage has peaks also in the middle of layer. Some of the amplitudes of these mid-layer peak points are comparable to the value at the layer edge.

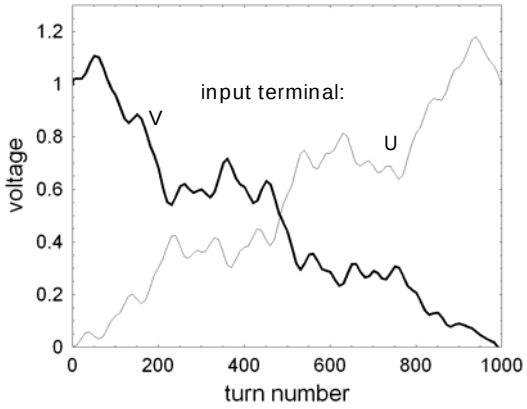

Fig. 6. Voltage distribution in the case that 1 MHz sinusoidal voltage is applied to Model C (number of groups: 100).

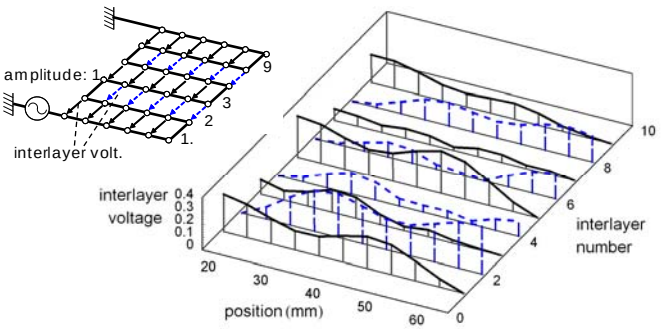

Fig. 7. Interlayer voltage distribution in the case that 1 MHz sinusoidal voltage is applied to terminal V of Model C (number of groups: 100).

VI. Time Domain Analyses

A. Response to step voltage

The response to a step voltage is calculated using the inverse FFT technique. In the analysis, a chopped input voltage is used as shown in Fig. 8. The induced voltage obtained by inverse FFT should subside within the period *T*. The time before chopping can be regarded as "observation period" for the induced voltage.

Fig. 9 shows voltages induced in various points of winding when a step voltage is applied to the terminal V of Model C. It is noticed that the transients comprise both fast and slow components. The latter continues longer than 1 μs.

The above result is rearranged as voltage distributions in Fig. 10. The oscillation phenomenon is quite similar to the voltage oscillation having been observed in transformers [2]. The initial voltage distribution (0 μs) is very much like the

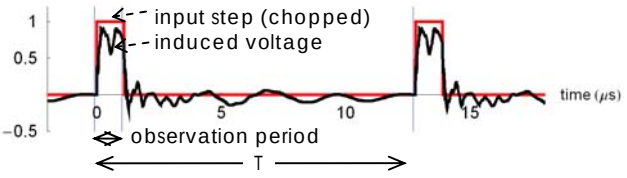

Fig. 8. Method to obtain induced voltage by inverse FFT (Voltage of 200th turn in Model C induced by a step applied at terminal V, number of groups: 100, T = 12.8 μs).

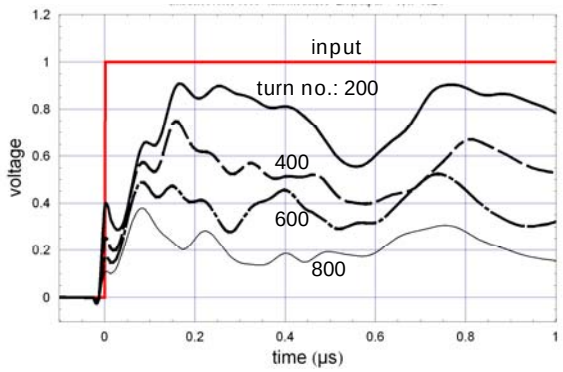

Fig. 9. Voltage induced in various points for step voltage input (Model C, terminal V, number of groups: 100, T = 12.8 μs).

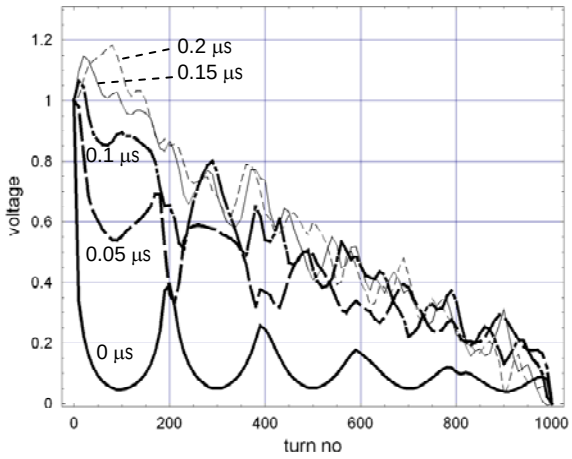

Fig. 10. Voltage distributions at different times for step voltage input (Model C, terminal V, number of groups: 100, T = 12.8 μs).

capacitive voltage distribution (see Fig. 13). The voltage distribution tends to a linear distribution gradually within a microsecond.

B. Impulse induced voltages

Interlayer voltages at layer edges (the positions shown by the arrows in Fig. 2) are calculated for Model A subjected to an impulse, and compared with experimentally obtained waveforms. The result is shown in Fig. 11 for the case that an impulse of 100 ns rise time is applied to terminal V. Only the interlayer voltages near to terminals are shown. The analysed and experimental agree fairly well. There is a tendency that the voltage is largest at the interlayer closest to terminal V (no.1) although some amount is also induced near terminal U (no.42).

The induced interlayer voltage depends on the waveform of applied voltage. Fig. 12 shows how the impulses of different rise times influence the voltage induced in interlayer no.1 of Model A. The voltage waveforms obtained analytically are similar to experimental, but the magnitude is slightly larger. Both the analysis and the experiment show that the induced voltage increases with the impulse rise time.

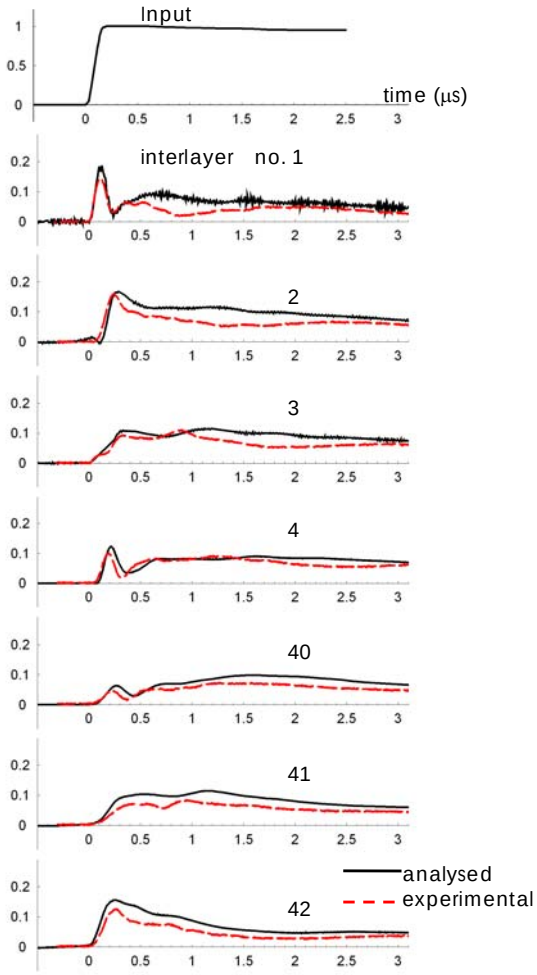

Fig. 11. Interlayer voltages induced by impulse of 100ns rise time (Model A, terminal V, number of groups in analysis: 1031).

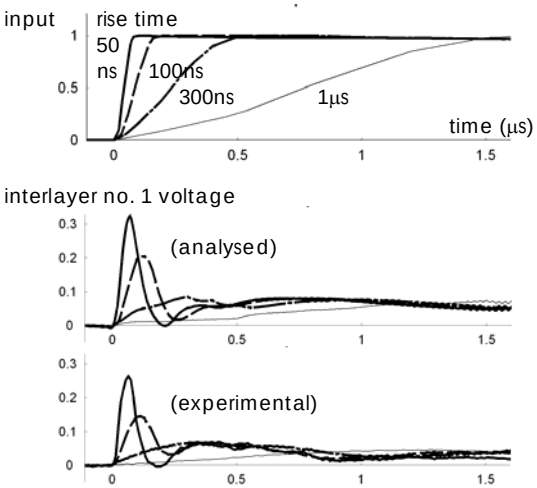

Fig. 12. Influence of impulse waveform on induced interlayer voltage (Model A, terminal V, number of groups in analysis: 2062).

VII. DISCUSSIONS

Implementing the proximity effect into the model, the present simulation gives better results than the previous report [3] both in frequency and time domain analyses.

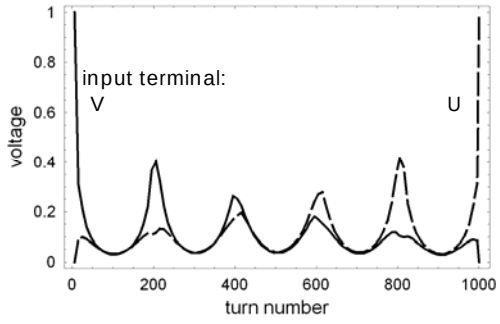

Fig. 13. Capacitive voltage distributions for Model C (number of groups: 100).

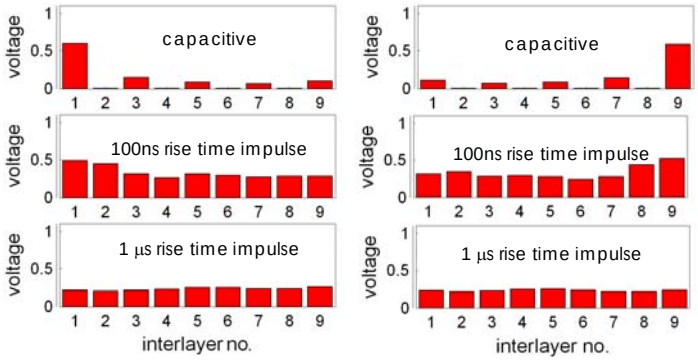

(a) input: V (b) input: U

Fig. 14. Induced interlayer voltage levels (peaks) in Model C for different impulses (number of groups: 100).

The non-uniformly induced voltage originates from the capacitive voltage distribution in the HV winding. Fig. 13 shows the capacitive voltage distributions for Model C in the two terminal cases V and U.

Fig. 14 shows the induced interlayer voltage levels in Model C. The top graphs are capacitive voltage levels corresponding to Fig. 13. The interlayer closest to application terminal is disproportionately highly stressed. The tendency is seen in the case of 100 ns rise time impulse as well. However, the voltage levels are almost the same in the case of 1 μs rise time. This is also confirmed in Model A and other actual VTs, although the induced levels are much lower than shown in Fig. 14. The reason is that the total numbers of layers in actual VTs are much larger than Model C.

The different effects of fast and slow impulses can be explained referring to the attenuation seen in the oscillation shown in Figs. 9 and 10, in which high frequency oscillations decay faster than those of low frequency. The cause of increased attenuation at high frequencies is that the proximity effect is pronounced at higher frequencies.

VIII. Conclusions

The high frequency model of VT having a large number of turns is constructed based on lumped constant circuit. The constants are calculated from the geometrical specifications of winding. The practical approximations have enabled implementing the proximity effect. The frequency characteristics and the time domain results obtained by inverse FFT method show a reasonable agreement with experimental. It is found that the interlayer insulation near to the impulse applied terminal tends to be stressed disproportionally, although the effect is less substantial in slower impulses.

The authors hope that the present method contributes to a better understanding of high frequency phenomena in VT and a rational insulation design of VTs concerning fast transients.

IX. References

[1] "Statistics of electricity safety in 2004," (in Japanese), *Japanese Nuclear and Industrial Safety Agency Homepage*, 2005, [Online]. Available: http://www.nisa.meti.go.jp/8_electric/setsubi_jiko.html

[2] A. Greenwood, *Electric transients in power systems* (2nd ed.), John New York: Wiley & Sons, 1991, pp.322-349.

[3] Y. Shibuya, K. Wada, and H. Muto, "Analysis of high frequency oscillations in voltage transformer," (in Japanese), *IEE of Japan Trans. B*, Vol.126, No.12, pp.1289-1294, 2006

[4] Y. Shibuya, T. Matsumoto, and T. Teranishi, "Modelling and analysis of transformer winding at High Frequencies," in *2005 International Conference on Power Systems Transients*, Paper No. IPST 05-025-3b

[5] F. de Leon, and A. Semlyen: "Detailed modeling of eddy current effects for transformer transients", IEEE Transactions on Power Delivery, Vol.9, No.7, pp.1143 - 1150, 1994

[6] D. J. Wilcox, "Theory of transformer modelling using modal analysis," *Proc. IEE, C* ,Vol.138, No.2, pp. 121-128, 1991

[7] Y. Shibuya, and S. Fujita, "High frequency model of transformer winding," (in Japanese), *IEE of Japan Trans. B*, Vol.123-B, No.2, pp.201-207, 2003

X. Biographies

Yoshikazu Shibuya was born in 1941. He graduated from Kyoto University in 1964. He received MS from Kyoto University and PhD from University of Salford, UK, in 1966 and 1974, respectively.
He was with Central Research Laboratory, Mitsubishi Electric Corporation from 1966 to 1999. His field is the fundamental insulation technology of various high voltage power apparatuses such as GIS and transformer. He is a professor at Shibaura Institute of Technology since 1999. Dr Shibuya is a fellow of IET and a member of IEE of Japan.

Kotaro Wada was born in 1974. He graduated from Tokyo Institute of Technology in 1996. He received MS from Tokyo Institute of Technology in 1998. He joined Mitsubishi Electric Corporation in 1998. Since then, he has been engaged in researches on insulation systems and surges in inverter, motor, and power apparatuses.

Hirotaka Muto graduated from Nagoya University in 1983. He received MS from Nagoya University in 1985. He joined Mitsubishi Electric Corporation in 1985. Since then, he has been engaged in developing insulation systems of motor, power electronics such as inverters, and power modules. He received PhD from Nagoya University.